ASEG2024
HOBART

A decade-long between-system comparison of AEM conductivities at Menindee Lake using deterministic and stochastic inversion.

Anandaroop Ray
Geoscience Australia
anandaroop.ray@ga.gov.au

Alan Yusen Ley-Cooper
Geoscience Australia
yusen.leycooper@ga.gov.au

Francesco Dauti
University of Milan, EEM Team
francesco.dauti@unimi.it

Ravin N. Deo
Geoscience Australia
ravin.deo@ga.gov.au

Sebastian Wong
Geoscience Australia
sebastian.wong@ga.gov.au

Ross C. Brodie
Formerly at Geoscience Australia

SUMMARY

Airborne electromagnetic (AEM) surveying provides a rapid means of imaging shallow subsurface geology as represented by changes in electrical conductivity within the earth. Aircraft-borne systems fly at different heights and with different speeds, and the exciting transients for time-domain AEM systems provide different spectral content to image the earth with. Geoscience Australia operates a test range over one of the Menindee lakes, in New South Wales, Australia, where different AEM systems have been flown over nearly a decade. Due to well studied geology and downhole induction data available in the area, this test range provides a useful proving ground for new AEM technology. For every test survey, certain lines within the range are repeatedly flown, and high-altitude lines are also acquired, such that robust data noise statistics can be established for all overflying AEM systems.

Test-range data and noise for various systems naturally allows us to compare AEM derived subsurface images of the test line. This study presents the results of both deterministic as well as Bayesian stochastic inversion over the same 13 km stretch of land, with six different systems flown between 2014-2023. While a deterministic inversion provides a first-pass image for comparing AEM systems, far more information is provided by the full posterior distribution of inverted conductivities, and in particular, the marginal quantiles of median and extremal conductivities over the entire image section.

Our findings indicate that there is generally good agreement with borehole logs, and the posterior conductivities for all systems agree well at the regional scale. The uncertainty (or the lack thereof) around ambiguous features in deterministic inversions is revealed through the stochastic inversions. Finally, we note that examination of water volumes in Menindee lakes do not show a simple relationship with inferred conductivity, indicating that unentangling environmental factors and system differences is a non-trivial matter.

Key words: Airborne electromagnetics; inversion; stochastic; Menindee; test-range

INTRODUCTION

Airborne electromagnetic surveys are routinely used for a multitude of purposes, ranging from the identification of mineralised conductors and host rocks, to geotechnical surveying, as well as regional stratigraphic mapping and groundwater assessment (e.g., Brodie, 2010; Auken et al., 2017; Ley-Cooper et al., 2020). For testing different AEM systems, it is therefore imperative to carry out quantitative inversion of acquired AEM transients, instead of qualitative comparisons of transient data, over areas of reasonably known geological structure and conductivity (Figure 1). Further, while quantitative inversions of AEM transients can be robustly and effectively carried out in a deterministic fashion, the nonlinear, ill-posed and non-unique nature of the AEM inverse problem necessitates the use of regularisation techniques to invert a stable, interpretable model (e.g., Constable et al., 1987; Farquharson and Oldenburg, 1998). The use of regularisation however, has inherent in it, certain disadvantages. For instance, some regularisation schemes force a return to a background "prejudice" model (e.g., Key, 2016) when sensitivity to the data are lost, and the smoothest possible model to fit the data, though a wise interpretational choice, is an extremal model. Probabilistic or stochastic inversions, when carried out with appropriate prior information, provide an ensemble of posterior models that are compatible with both the prior information, as well as the observed data and its noise statistics. This in turn reduces the uncertainty of geological interpretation, and makes comparisons between AEM systems over the same stretch of land easier.

INVERSION APPROACHES

A deterministic as well as probabilistic approach was used to invert data from all systems using the HiQGA (Ray et al., 2023) codebase (v0.4.6), with identical hyper-parameter settings, priors and 52-layer model parameterisation. For the deterministic inversions, a fast Occam approach (Key, 2016) was used, where the following objective function is minimised:

$$\phi(\mathbf{m}) = \frac{1}{2}\left(||\mathbf{W}(\mathbf{d} - \mathbf{f}(\mathbf{m}))||^2 + \lambda^2 \left[||\mathbf{R}\mathbf{m}||^2 + \beta^2 ||\mathbf{m} - \mathbf{m_0}||^2 \right] \right). \quad (1)$$

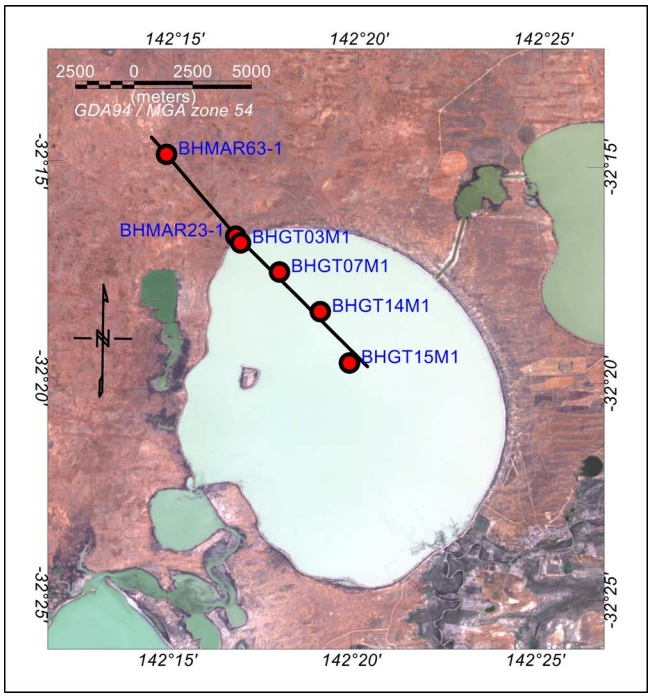

Figure 1. The Menindee test range in New South Wales, Australia (after Ray et al., 2023). The repeat section with a number of boreholes (red and black circles) intersecting the line is shown here.

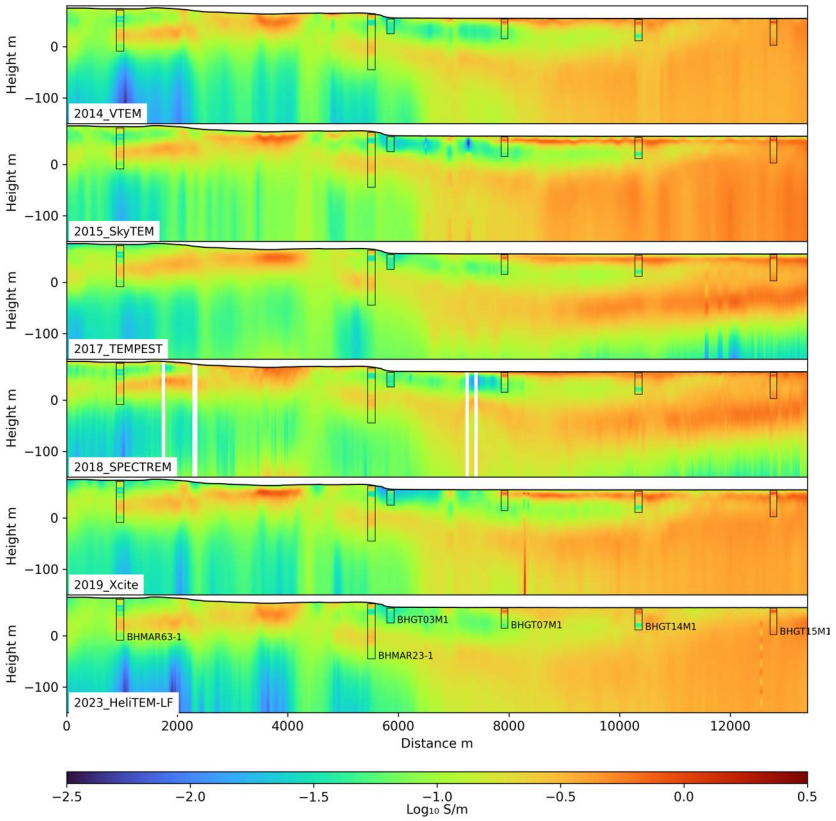

Figure 2. Deterministic inversions for six systems arranged chronologically from top to bottom. Also shown are induction logs in the same colour scale.

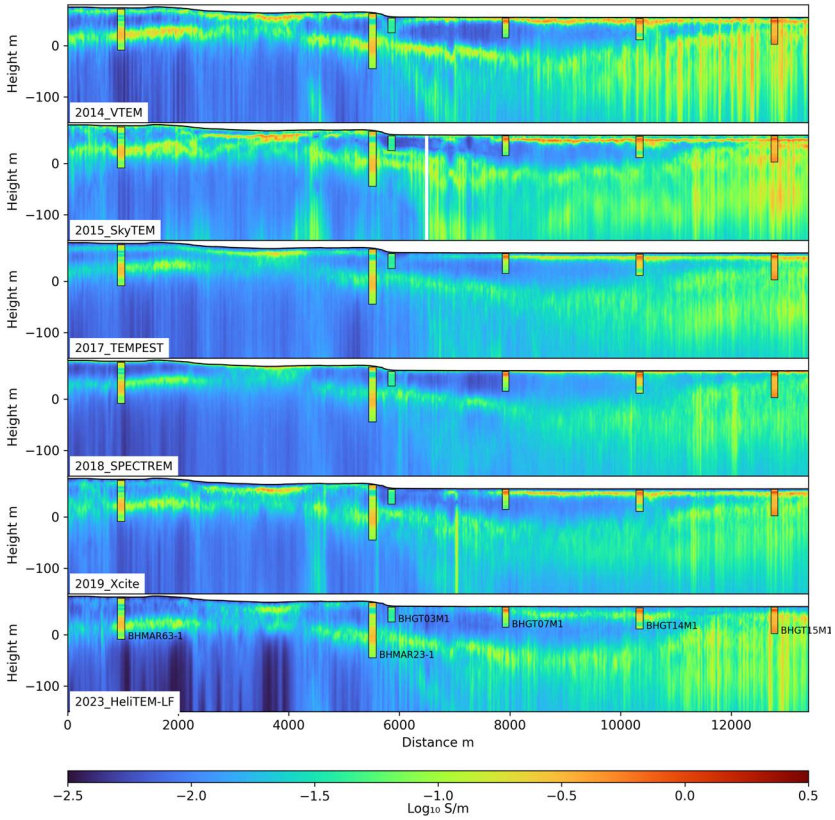

Figure 3. The 10th (low) percentile of conductivity. Note how conducting geology stands out in this percentile. Low percentile values should generally be lower than those in the wells.

The AEM forward operator is $\mathbf{f}$, and data are contained in $\mathbf{d}$. $\mathbf{W}$ are data weights such that $\mathbf{W}^t\mathbf{W}$ is the inverse data covariance matrix $\mathbf{C}_d^{-1}$, and conductivities are represented by the model $\mathbf{m}$. λ^2 is the trade-off parameter, $\mathbf{R}$ is a first or second differences operator, and $\mathbf{m_0}$ is the reference model. λ^2 is found by sweeping through a decreasing range of positive values until the misfit $||\mathbf{W}(\mathbf{d}-\mathbf{f}(\mathbf{m}))||^2$ from the model in the last iteration decreases to 0.7 of its previous value. In the second stage, when enough iterations have been run such that misfit is underneath the data noise, root finding is used to find the largest λ^2 that returns a model at the target AEM data noise. This ensures that the smoothest model compatible with the observations is attained. However, the choice of β^2, another positive quantity, is left to the user. Large β^2 values ensure a quicker return to the reference model, while fractional values pay more attention to minimising model roughness. For fixed-wing systems, transmitter-receiver geometry nuisances are inverted in an alternate step with a BFGS scheme (Nocedal and Wright, 2006).

For the probabilistic inversions, we use a Bayesian approach:

$$p(\mathbf{m}|\mathbf{d}) \propto p(\mathbf{d}|\mathbf{m}) \cdot p(\mathbf{m}), \tag{2}$$

where $p(\mathbf{m})$ is the prior model probability, $p(\mathbf{d}|\mathbf{m})$ is the model likelihood obtained from the model misfit and data noise statistics, and $p(\mathbf{m}|\mathbf{d})$ is the posterior probability inference we are after, which weights the misfit and the prior knowledge proportionately. We use the trans-dimensional Gaussian process inversion scheme (Ray and Myer, 2019; Ray, 2021) together with the modifications for marginalising fixed-wing geometry nuisances provided in Ray et al. (2023).

COMPARITIVE SECTIONS

Six different systems are compared, both deterministically and probabilistically. For each system, noise levels are determined from variance in repeat flights, as well as in high altitude flights. These are then added in quadrature as two independent noise sources (Green and Lane, 2003).

Deterministic results

All models were inverted with identical $\beta^2 = 0.0001$, ensuring only a weak adherence to the background reference conductivity $\mathbf{m_0} = 0.01$ S/m. The results are shown in Figure 2. Qualitatively, the degree of similarity between the induction logs and inverted

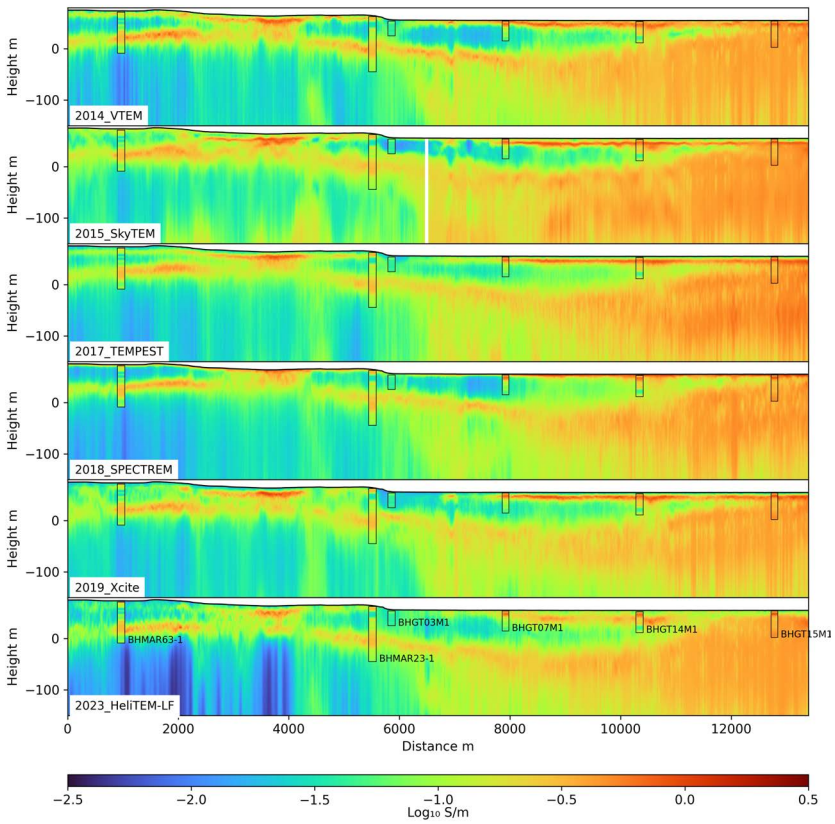

Figure 4. The 50th (median) percentile of conductivity. This presents a "middle of the road" view of the subsurface geology. Median conductivity values should be in the vicinity of those in the wells.

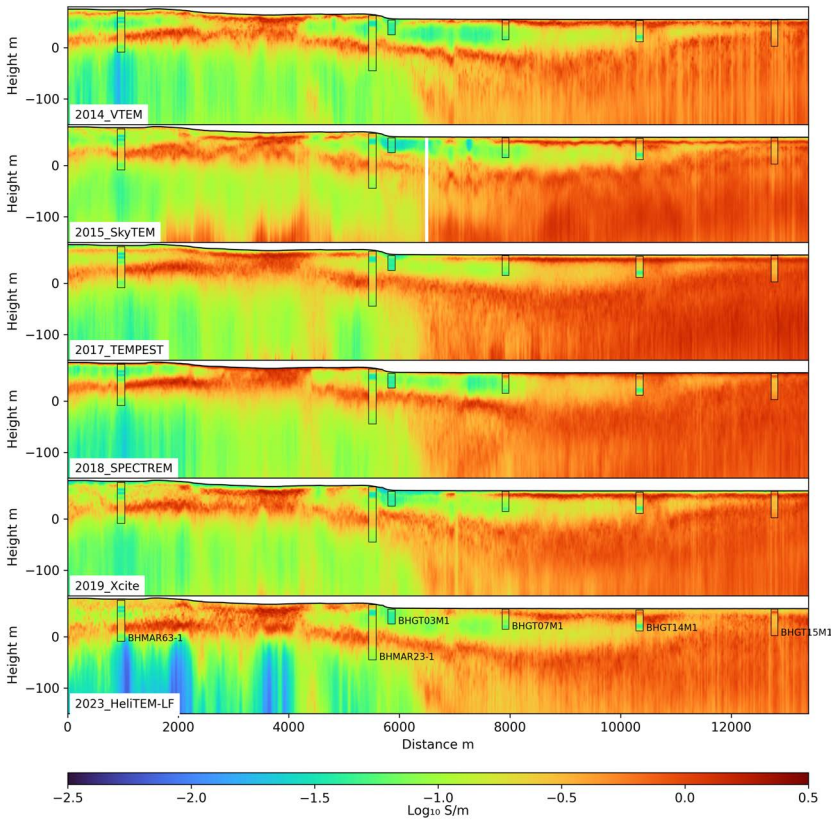

Figure 5. The 90th (high) percentile of conductivity. High percentile values should generally be higher than those in the wells.

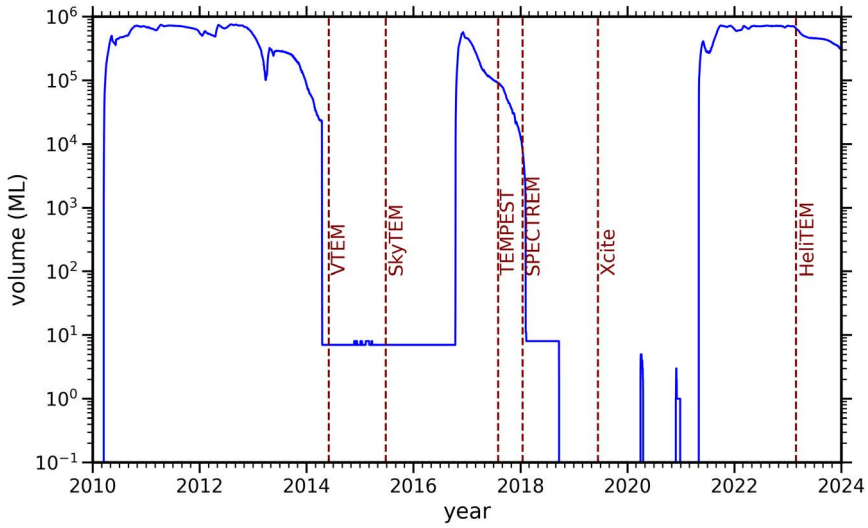

Figure 6. Water volume as obtained from monitoring site 425022, which feeds the water from the Darling river to Lake Menindee. Despite massive changes in reservoir water volume due to local and eastern seaboard rain events, only subtle changes in conductivity are seen in both the deterministic as well probabilistic AEM imaging results in Figures 2–5.

conductivity at the same location is remarkable, given that the induction logs were acquired between 2008-2010. Inverted conductivities for soundings with root mean square error > 1.5 have been blanked. Both the fixed-wing systems (TEMPEST, SPECTREM) have been inverted with the amplitude of the $\mathbf{B}$ field in the in-line receiver plane. It is unclear from the eastern part of the section (8 km along line onwards), whether the fixed-wing systems have recovered resistive background (blue) at depth, or are returning to the background values due to a loss in sensitivity.

Probabilistic results

All models were inverted with identical prior ranges for subsurface conductivities as well as geometry nuisances (for fixed wing surveys). The results are shown in Figures 3, 4, and 5. As earlier, the fixed-wing systems were inverted with the amplitude of the $\mathbf{B}$ field. Again, quite remarkably, the logged induction downhole conductivities generally fall in-between the inferred low and high percentiles, despite the amount of time that has elapsed between the logging and the acquisition. For a particular system, a low spread of conductivity between percentiles indicates low posterior uncertainty and vice versa. Note how it is now possible to infer that the western part of the section (2 km along line) is indeed resistive below 0 m height, while between 8 to 10 km along the line, we encounter from surface to depth, a conductive-resistive-conductive sequence which becomes highly uncertain deeper than -50 m height.

Comparison with reservoir water volume

Water volume data were acquired from monitoring site (425022) at Sunset Strip, which feeds the water from the Darling river to Lake Menindee. The results are illustrated in Figure 6. Examining the deterministic AEM sections, as well as the probabilistic percentiles (Figures 2–5), the changes in subsurface geology with time do not appear to be very obviously related with the volumes of water in the reservoir.

CONCLUSIONS

Nearly a decade of AEM data over the Menindee test range have been inverted deterministically as well as stochastically. While the probabilistic inversions reduce interpretation ambiguity, all subsurface images are quite similar at the regional scale. Subtle differences in the conductivity sections and percentiles cannot easily be linked with changes in water volume in the lake, despite massive rainfall events having occurred over the years. This implies that careful attention to system repeatability, as well as contemporaneous ground truthing and ground geophysical acquisition is required, before AEM systems can be used reliably for time lapse purposes.

ACKNOWLEDGMENTS

Geoscience Australia thanks the geophysical contractors who fly the test range at Geoscience Australia's request. We also thank the Geological Survey of New South Wales for fruitfully collaborating to establish the test range. This abstract is published with the per-

mission of the CEO, Geoscience Australia.

The HiQGA codebase was developed within the Australia's Resources Framework project as part of the Exploring for the Future Program, and is available from `https://github.com/GeoscienceAustralia/HiQGA.jl`.

REFERENCES

Auken, E., Boesen, T., and Christiansen, A. V., 2017, A review of airborne electromagnetic methods with focus on geotechnical and hydrological applications from 2007 to 2017:, volume 58 Elsevier Inc., 1 edition.

Brodie, R. C., 2010, Holistic inversion of airborne electromagnetic data:, pages 121–127.

Constable, S. C., Parker, R. L., and Constable, C. G., 1987, Occam's inversion: A practical algorithm for generating smooth models from electromagnetic sounding data: Geophysics, **52**, 289–300.

Farquharson, C. G., and Oldenburg, D. W., 1998, Non-linear inversion using general measures of data misfit and model structure: Geophysical Journal International, **134**, 213–227.

Green, A., and Lane, R., 2003, Estimating noise levels in aem data: ASEG Extended Abstracts, **2003**, 1–5.

Key, K., 2016, Mare2dem: A 2-d inversion code for controlled-source electromagnetic and magnetotelluric data: Geophysical Journal International, **207**, 571–588.

Ley-Cooper, A. Y., Brodie, R. C., and Richardson, M., 2020, Ausaem: Australia's airborne electromagnetic continental-scale acquisition program: Exploration Geophysics, **51**, 193–202.

Nocedal, J., and Wright, S. J., 2006, Numerical optimization: Springer.

Ray, A., and Myer, D., 2019, Bayesian geophysical inversion with trans-dimensional gaussian process machine learning: Geophysical Journal International, **217**, 1706–1726.

Ray, A., Ley-Cooper, Y., Brodie, R. C., Taylor, R., Symington, N., and Moghaddam, N. F., 7 2023, An information theoretic bayesian uncertainty analysis of aem systems over menindee lake, australia: Geophysical Journal International, **235**, 1888–1911.

Ray, A., 2021, Bayesian inversion using nested trans-dimensional gaussian processes: Geophysical Journal International, **226**, 302–326.